J. Fluid Mech. (1983), *vol.* 131, *pp.* 305–317
Printed in Great Britain

The calculation of separation bubbles in interactive turbulent boundary layers

By TUNCER CEBECI
Mechanical Engineering Department, California State University, Long Beach, California
AND SUZANNE M. SCHIMKE
Aerodynamics Research Department, Douglas Aircraft Company, Long Beach, California

(Received 11 October 1982)

A viscous–inviscid interaction procedure is presented for computing incompressible separation bubbles in two-dimensional flows. The analysis consists of the solution of the inviscid-flow equations with a conformal-mapping method and the solution of the boundary-layer equations with an inverse procedure. The boundary-layer equations employ the Cebeci–Smith algebraic eddy-viscosity formulation. The coupling between the inviscid and boundary-layer equations is established through the Hilbert integral by using Veldman's suggestion. An empirical method is used to calculate the location of transition, which is found to play a key role in predicting the behaviour of separating flows. Numerical solutions are presented for transitional bubbles on an NACA 66_3-018 airfoil at two angles of attack for a chord Reynolds number of 2×10^6. Comparisons wth experiment show that the flow properties of the separation bubbles can be predicted very well with this procedure provided that an accurate estimate of transition location is made.

1. Introduction

According to experiment, one form of airfoil stall stems from local regions of separated flow which originate when a laminar boundary layer separates from a surface. In the early stages of stall when the flow does not completely separate, transition to turbulent flow takes place in the detached boundary layer a short distance downstream from separation, and the flow is subsequently reestablished on the surface as a turbulent boundary layer. The region between the laminar separation and turbulent reattachment is commonly termed the 'laminar-separation bubble'.

The appearance of bubbles on airfoils often signifies that the airfoils are about to stall and this, in turn, may be associated with the bursting of the bubbles. The review of bubble separations by Tani (1964) is still a valuable starting point for any investigation. He showed that the sequence of events from the first appearance of separation on the upper surface to the bursting of the bubble is complicated and is particularly dependent on the geometric properties of the airfoil and the chord Reynolds number R_c. Although bubbles may be found on thin airfoils near the leading edge (short bubbles), they have also been observed near midchord on comparatively thick airfoils (long bubbles) for angles of attack near 0° (see Burshall & Loftin 1951; Gault 1955). For short bubbles, it is necessary that R_c not be too small, otherwise laminar separation, when it occurs, will not be followed by reattachment; at higher values of R_c, transition occurs in the separated boundary layer, which then reattaches as a turbulent boundary layer. With an increase in the angle of attack, separation

moves towards the leading edge and eventually the bubble bursts without reattachment of the turbulent boundary layer causing the airfoil to stall. In the case of long bubbles, the Reynolds number is sufficiently large so that, if there is laminar separation, transition occurs in the separated boundary layer, which then reattaches as a turbulent boundary layer.

Since Tani's review, there have been several experimental studies throwing additional light on the bubble properties, the most recent being that of Arena & Mueller (1980). On the theoretical side an important contribution was made by Briley & McDonald (1975), who used both an interactive boundary-layer approach and a Navier–Stokes theory. Kwon & Pletcher (1979) have tackled similar problems using an interactive boundary-layer approach and allowing the displacement thickness to modify the external velocity. Both of these studies concentrated on the calculation of long bubbles and made some use of the measured pressure distribution on the airfoil. The study conducted by Crimi & Reeves (1976), on the other hand, examined the calculation of short bubbles using an integral method which included the effects of viscous–inviscid interaction. The separated laminar shear layer, transitional flow and turbulent reattaching flow are represented in their method, and solutions were obtained using an iterative procedure with strong interaction effects limited to the immediate vicinity of the separation bubble.

In this paper we consider the calculation of long bubbles by using an interactive boundary-layer theory and present results for conditions which correspond to the measurements of Gault (1955) in the flow around an airfoil at 0° and 2° angle of attack. Standard and inverse boundary-layer procedures, with an algebraic eddy-viscosity formulation, are interacted with perturbations of the potential-flow solutions found using the conformal-mapping method of Halsey (1979). The calculated and measured results are compared, and experiences with the use and interaction of the numerical methods together with the accuracy of a turbulence model, including the transitional region, are described and discussed.

2. Governing equations

For two-dimensional steady incompressible flows, the boundary-layer equations are well known, and, with the eddy viscosity (ϵ_m) concept, they can be written in the form

$$\frac{\partial u}{\partial x}+\frac{\partial v}{\partial y}=0, \tag{1}$$

$$u\frac{\partial u}{\partial x}+v\frac{\partial u}{\partial y}=u_e\frac{\mathrm{d}u_e}{\mathrm{d}x}+\frac{\partial}{\partial y}\left(b\frac{\partial u}{\partial y}\right), \tag{2}$$

where $b=\nu+\epsilon_m$. In the absence of mass transfer, (1) and (2) are subject to boundary conditions given by

$$\left.\begin{aligned} u=v=0 \quad (y=0),\\ u=u_e(x) \quad (y=\delta). \end{aligned}\right\} \tag{3}$$

In (3), the external velocity distribution $u_e(x)$ is obtained either from experiment or from inviscid flow theory. In the latter case it is often necessary to consider the effect of the boundary layer on the calculated external velocity distribution and this can be done in several ways. The procedure used here and by Veldman (1979) and by Cebeci, Stewartson & Williams (1980) is to write the edge-boundary condition,

with $u_e^0(x)$ denoting the inviscid velocity distribution and $u_c(x)$ the perturbation velocity due to the viscous effects, as

$$u_e(x,\delta) = u_e(x) = u_e^0(x) + u_c(x) \tag{4}$$

and compute u_c from the Hilbert integral

$$u_c(x) = \frac{1}{\pi}\int_{-\infty}^{\infty} \frac{\mathrm{d}}{\mathrm{d}\sigma}(u_e\delta^*)\frac{\mathrm{d}\sigma}{x-\sigma}, \tag{5a}$$

where $(\mathrm{d}/\mathrm{d}x)(u_e\delta^*)$ is the blowing velocity used to simulate the boundary layer.

We assume that the effect of the bubble is local, so that the interaction region is limited to a finite range $x_a \leqslant x \leqslant x_b$. This allows us to rewrite (5*a*) as

$$u_c(x) = \frac{1}{\pi}\int_{x_a}^{x_b} \frac{\mathrm{d}}{\mathrm{d}\sigma}(u_e\delta^*)\frac{\mathrm{d}\sigma}{x-\sigma}. \tag{5b}$$

Following Veldman (1979) and Cebeci *et al.* (1980), we write (4) and (5*b*) as

$$u_e(x,\delta) = u_e^0(x) + \sum_{j=1}^{n} c_{ij}(u_e\delta^*)_j. \tag{6}$$

Here c_{ij} denotes the interaction-coefficient matrix, which is obtained from a discrete approximation to the Hilbert integral in (5*b*). In this form, (6) provides an outer boundary condition for the viscous-flow calculation which represents the viscous/inviscid interaction.

2.1. *Turbulence model*

The presence of the eddy viscosity ϵ_m requires a turbulence model; in our study we use the algebraic eddy-viscosity formulation developed by Cebeci & Smith (1974). According to this formulation, ϵ_m is defined by two separate formulas. In the so-called inner region of the boundary layer $(\epsilon_m)_i$ is defined by

$$(\epsilon_m)_i = \left\{0.4y\left[1-\exp\left(\frac{-y}{A}\right)\right]\right\}^2\left|\frac{\partial u}{\partial y}\right|\gamma_{tr} \quad (0 \leqslant y \leqslant y_c), \tag{7}$$

where

$$A = 26\nu u_\tau^{-1}[1-11.8p^+]^{-\frac{1}{2}}, \quad u_\tau = \left(\frac{\tau}{\rho}\right)_{\max}^{\frac{1}{2}}, \quad p^+ = \frac{\nu u_e}{u_\tau^3}\frac{\mathrm{d}u_e}{\mathrm{d}x}. \tag{8}$$

In the outer region $(\epsilon_m)_o$ is defined by

$$(\epsilon_m)_o = \alpha\int_0^{\infty}(u_e-u)\,\mathrm{d}y\,\gamma_{tr} \quad (y_c \leqslant y \leqslant \delta). \tag{9}$$

Here α is a constant equal to 0.0168. The condition used to define the inner and outer regions is the continuity of the eddy viscosity; from the wall outward $(\epsilon_m)_i$ is applied until $(\epsilon_m)_i = (\epsilon_m)_o$, which defines y_c.

In (7) and (9) γ_{tr} is an intermittency factor that accounts for the transitional region that exists between a laminar and turbulent flow. Several expressions are available for this purpose, and here we have chosen that suggested by Chen & Thyson (1971). It is given by

$$\gamma_{tr} = 1-\exp\left[-G(x-x_{tr})\int_{x_{tr}}^{x}\frac{\mathrm{d}x}{u_e}\right]. \tag{10}$$

Here x_{tr} is the location of the start of transition, and the empirical factor G is given by

$$G = \frac{1}{1200}\frac{u_e^3}{\nu^2}R_{x_{tr}}^{-1.34}. \tag{11}$$

The transition Reynolds number is defined as $R_{x_{tr}} = (u_e x/\nu)_{tr}$. Equation (10) assumes that the extent of the transitional region, with subscript t denoting the end of the transition region, is

$$x_t - x_{tr} = \frac{60x_{tr}}{R_{x_{tr}}^{0.33}}. \tag{12a}$$

In terms of Reynolds number, (12a) can also be written as

$$R_{\Delta x_{tr}} = 60R_{x_{tr}}^{0.67}. \tag{12b}$$

Equation (10) is based on empirical data in which transition from laminar to turbulent flow takes place naturally, that is without tripping the boundary layer or without flow separation. How good it is for flows in which transition is caused by laminar-flow separation needs to be explored, as we shall see later in the paper.

2.2. *Transition prediction*

The solution of (1) and (2) requires the specification of the transition point, and empirical methods can be used for this purpose. That described by Cebeci & Bradshaw (1977) agrees with the predictions of the e^9 method and is given by

$$R_{\theta_{tr}} = 1.174\left[1 + \frac{22400}{R_{x_{tr}}}\right]R_{x_{tr}}^{0.46}. \tag{13}$$

This correlation formula works reasonably well for flows in which transition is upstream of flow separation. However, if the separation precedes transition, then the solution of the boundary-layer equations break down, owing to the singular nature of the equations at separation, when the external velocity is given and (13) cannot be used. As a result, the laminar separation point is often taken to be the transition point. In general this is a useful assumption, but it has the drawback that it assumes transition to be independent of the Reynolds number in a separating flow. Kwon & Pletcher (1979) overcome the difficulty about the singularity by solving the equation in the inverse mode and are thereby able to use (13) in the post-separation zone. As we shall see, the specification of transition point in such flows is a matter of some delicacy so far as computations are concerned, a slight error leading to substantial changes in the flow field. The formula (13) is rather insensitive to x_{tr} because θ changes only slowly in this region. Kwon & Pletcher appeared to fix transition with their first estimate of δ^*, which implies that they have to rely to some extent on experimental evidence.

An alternative procedure for predicting transition in a bubble is to assume that the mechanism is similar to that occurring downstream of an element of surface roughness. In such a situation the flow separates at the roughness element and reattaches further downstream. The separated flow is initially laminar and less stable than an attached boundary layer, so that transition is triggered there. Based on this hypothesis Crimi & Reeves (1976) recommended the relation

$$\frac{y_{u=0}}{\delta_s^*} = \frac{10^6}{(u_e\delta^*/\nu)_s^2} \tag{14}$$

for computing the transition location in a separation bubble near the leading edge.

Here $y_{u=0}$ represents the y-distance ($y > 0$) where the streamline velocity u vanishes, and the subscript s denotes the location of separation. In our calculations, we compute the right-hand side of (14) at the first x-location where the flow separates. At that station and at subsequent stations, we also compute the left-hand side of (14). Transition is assumed to occur when both expressions are equal. From a computational point of view (14) has the advantage that the onset of transition is defined more clearly since $y_{u=0}$ increases sharply downstream of separation.

3. Solution procedure

As in previous studies (see e.g. Bradshaw, Cebeci & Whitelaw 1981) we use similarity variables to transform the governing equations. This also allows us to start the calculations easily at the stagnation point and to take larger steps in the streamwise direction. With the definition of stream function ψ and Falkner–Skan transformation,

$$\eta = \left(\frac{u_e}{\nu x}\right)^{\frac{1}{2}} y, \quad \psi = (u_e \nu x)^{\frac{1}{2}} f(x, \eta), \tag{15}$$

(1)–(3) become

$$(bf'')' + \tfrac{1}{2}(m+1)ff'' + m[1-(f')^2] = x\left(f'\frac{\partial f'}{\partial x} - f''\frac{\partial f}{\partial x}\right) \tag{16}$$

$$\left.\begin{aligned} f = f' = 0 \quad (\eta = 0), \\ f' = 1 \quad (\eta = \eta_e). \end{aligned}\right\} \tag{17}$$

Here a prime denotes differentiation with respect to η, and m is a dimensionless pressure-gradient parameter defined by

$$m = \frac{x}{u_e}\frac{\mathrm{d}u_e}{\mathrm{d}x}. \tag{18}$$

We use this form of the equations to obtain the boundary-layer solution for a given pressure distribution, which for brevity we call the standard problem. When we solve the equations with the interactive viscous effects, an inverse method is used and we find it convenient to solve the equations expressed in primitive variables. With u_0 and L denoting a reference velocity and length respectively, we define dimensionless Y and stream function $F(x, Y)$ by

$$Y = \left(\frac{u_0}{\nu L}\right)^{\frac{1}{2}} y, \quad \psi = (u_0 \nu L)^{\frac{1}{2}} F(x, Y). \tag{19}$$

Equations (2) and (3), with a prime now denoting differentiation with respect to Y, become

$$(bF'')' + \bar{u}_e\frac{\mathrm{d}\bar{u}_e}{\mathrm{d}x} = F'\frac{\partial F'}{\partial x} - F''\frac{\partial F}{\partial x}, \tag{20}$$

$$\left.\begin{aligned} F = F' = 0 \quad (Y = 0), \\ F' = \frac{u_e}{u_0} = \bar{u}_e \quad (Y = Y_e). \end{aligned}\right\} \tag{21}$$

In terms of dimensionless quantities (denoted by bars), with D representing $Y_e F'_e - F$ (4) and (5b) can be written as

$$\bar{u}_e(x) = \bar{u}_e^0(x) + \frac{1}{\pi R_L^{\frac{1}{2}}}\int_{x_a}^{x_b}\frac{\mathrm{d}D}{\mathrm{d}\xi}\frac{\mathrm{d}\xi}{\bar{x}-\xi}. \tag{22}$$

As shown by Cebeci *et al.* (1980), (6) can be expressed in the dimensionless form

$$F'_e(x_i) - \tilde{C}_{ii} D(x_i) = g_i, \tag{23}$$

where $\tilde{C}_{ii} = c_{ii}/R_L^{\frac{1}{2}}$, x_i denotes the station x where the equations are being solved, and the known parameter g_i is given by

$$g_i = \bar{u}_e^0(x_i) + \sum_{k=1}^{i-1} \tilde{C}_{ik} D(x_k) + \sum_{k=i+1}^{l} \tilde{C}_{ik} DB(x_k). \tag{24}$$

Here $\tilde{C}_{ik}$ are the fixed interaction coefficients, whose evaluation is described by Cebeci *et al.* (1980).

An iterative solution procedure is employed in which successive sweeps of the boundary-layer calculation are performed using (23) and (24) to define the interaction between the viscous and the inviscid flow regimes. Thus, for any given sweep, $D(x_k)$ denotes the values computed for the current sweep, while $DB(x_k)$ denotes the values computed for the previous sweep.

To solve the equations for the standard and inverse problems we use Keller's box method, which is described in detail in several references (e.g. Bradshaw *et al.* 1981). The inverse procedure employing the Mechul function has also been described in the latter reference, and the following paragraph explains the numerical formulation.

According to the box method we first reduce (20)–(23) to a first-order system. With $\bar{u}_e$, F' and F''' represented by w, r and v respectively, we write

$$F' = r, \quad r' = v, \quad w' = 0, \tag{25a,b,c}$$

$$(bv)' + w\frac{\mathrm{d}w}{\mathrm{d}x} = r\frac{\partial r}{\partial x} - v\frac{\partial F}{\partial x}, \tag{25d}$$

$$F = r = 0 \quad (Y = 0), \tag{26a}$$

$$r_e = w_e, \quad r_e - \tilde{C}_{ii}(Y_e r_e - F_e) = g_i \quad (Y = Y_e). \tag{26b}$$

The numerical solution of the system given by (25) and (26) is described in Bradshaw *et al.* (1981). A feature to note is that *in* the recirculating region the convective term $r(\partial r/\partial x)$ is set equal to zero, following the FLARE approximation. Because the separation region is small, no attempt was made to improve the approximations resulting from that assumption.

4. Results

The evaluation of the method described in previous sections is made for the experimental data of Gault (1955), which were obtained on an NACA 66_3-018 airfoil. For two angles of attack, $\alpha = 0°$ and $2°$ at $R_c = 2 \times 10^6$, the data include pressure distributions and velocity profiles in the separated-flow region, which covers about 10 % chord, extending from $s/c = 0.62$ to 0.725 for $\alpha = 0°$ and from $s/c = 0.61$–0.715 for $\alpha = 2°$. Note that we now use s to denote surface distances in order to distinguish it from the chordwise distance x used for airfoils. At higher angles of attack, the separation bubble moves very close to the leading edge. In this case, the separation region is limited to about 2 % chord. Experimental data also contains separation and reattachment points as well as transition points at several chord Reynolds numbers.

The converged solutions were found to be very sensitive to the transition location used in the boundary-layer calculation. If the transition location is specified a short distance upstream of the laminar separation point, the size of the separation bubble

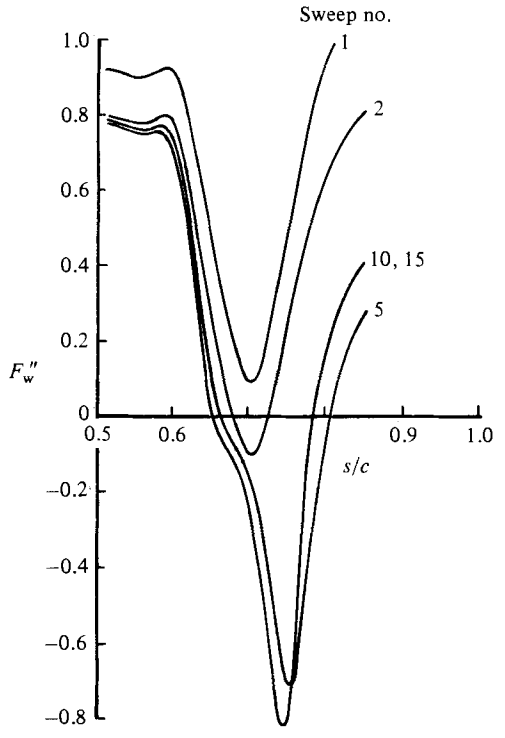

FIGURE 1. Variation of wall-shear parameter F_w'' with number of sweeps for $\alpha = 0$, $R_c = 2 \times 10^6$.

is reduced or eliminated entirely. However, if the transition location is specified a short distance downstream of this point, the separated region will grow with each sweep, and the solution will eventually break down. The empirical formula given by (14) has therefore been used to specify the transition location.

The calculations in our study were first made by computing the pressure distribution for the NACA 66_3-018 airfoil shape at a specified angle of attack by using Halsey's (1979) conformal-mapping method. Since the location of transition was not known prior to the boundary-layer calculations, solutions were first obtained for the specified inviscid pressure distribution by using the standard method: then transition was computed from (13). However, in the test cases considered in this paper, namely $\alpha = 0°$ and 2°, laminar separation took place before transition could be computed from that equation. Therefore transition was taken to be the laminar separation point for the first iterative sweep.

The subsequent iterations were performed by using the standard method from the stagnation point up to $s/c = 0.30$, at which point the inverse boundary-layer calculations were started and continued to the trailing edge. If a region of separated flow was found to exist, then the new location of transition was determined from (14); otherwise the laminar separation point was used. After the completion of this first sweep, the following sweeps utilized (14) until the solutions converged.

Figures 1 and 2 show the calculated and experimental results for $\alpha = 0°$. Figure 1 shows the computed wall-shear parameter F_w'' for several sweeps on the airfoil, and figure 2 allows comparison of calculated and experimental velocity profiles at different streamwise locations. From figure 1 we see that, in sweep 1 with transition corresponding to laminar separation, the inverse calculations do not contain a

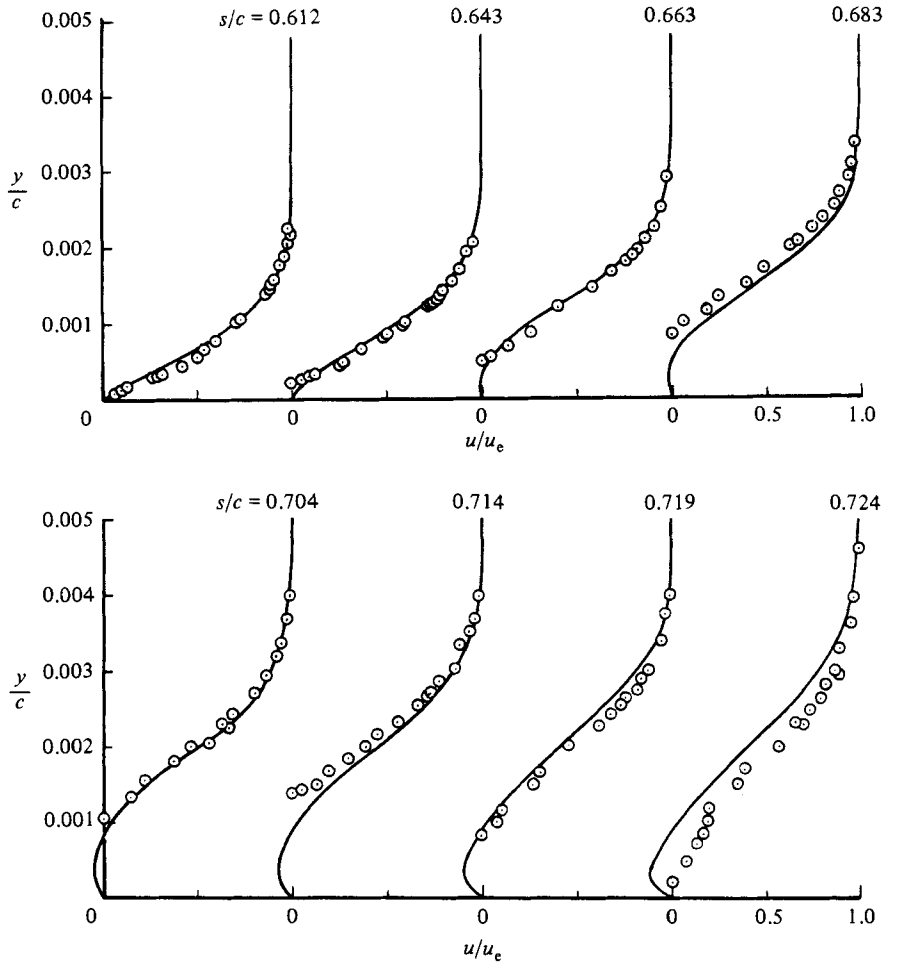

FIGURE 2. Comparison of calculated (solid line) and experimental (symbols) velocity profiles for $\alpha = 0$, $R_c = 2 \times 10^6$ after 15 sweeps.

separated region. However, in the second sweep, the calculations contain a small separated region with transition location still at $s/c = 0.66$, indicating that during that sweep (14) did not indicate any transition. The third set of calculations (not shown on the figure) contain a larger region of separated flow with transition location computed by (14) to be at $s/c = 0.69$. Table 1 presents the location of transition as a function of sweep number. It indicates that after sweep 6 the transition location remains unchanged at $s/c = 0.67$. Figure 1 also shows that the overall solution converges after about ten sweeps. According to the results of figure 2, the agreement between computed and measured velocity profiles is good, apart from the last streamwise station $s/c = 0.724$, where the calculations and experiment indicate different reattachment locations. This flow was also studied by Briley & McDonald (1975), who solved the full Navier–Stokes equations near the separation bubble using a one-parameter mixing-length profile, and by Kwon & Pletcher (1979), who, like us, used an interactive boundary-layer approach. In both studies the velocity profiles were essentially indistinguishable from ours, but the skin-friction coefficients differed significantly. The experimental position of separation and reattachment differ from

Sweep	$(s/c)_{tr}$
1	0.66 (laminar separation)
2	0.66
3	0.69
4	0.68
5	0.68
6–15	0.67

TABLE 1. Variation of transition location for different sweeps for $\alpha = 0°$

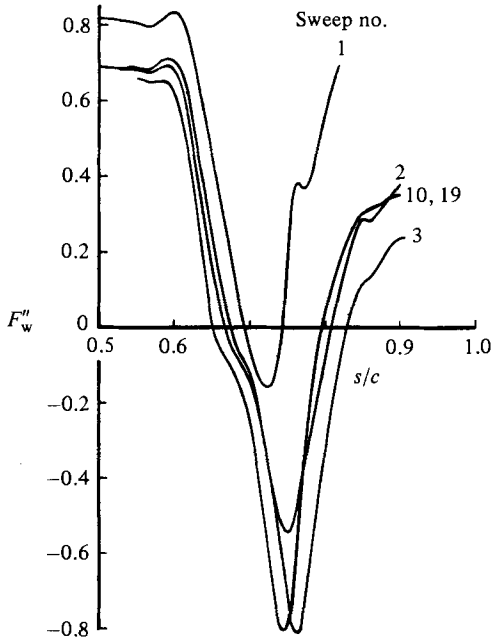

FIGURE 3. Variation of wall-shear parameter F''_w with number of sweeps for $\alpha = 2$, $R_c = 2 \times 10^6$.

the positions predicted by the theories and it is not possible to decide which is in the best agreement.

Figures 3 and 4 show comparisons similar to those in figures 1 and 2 for $\alpha = 2°$, and table 2 presents the location of transition as a function of sweep number. The agreement between calculated and experimental velocity profiles, as in the case of $\alpha = 0°$, is again very good except for the last station where the boundary layers attach. Again the transition location computed according to (14) settles down at $s/c = 0.67$, and remains unchanged with sweep number after ten streamwise iterations. We also note from figure 3 that the dip in wall shear is quite large with computed separation and reattachment points differing from those of measured ones.

Figures 5 and 6 show a comparison between calculated and measured pressure coefficients $1 - C_p$ for $\alpha = 0°$ and 2° respectively. Also shown in figure 5 is the pressure coefficient computed by Briley & McDonald. As is seen, the difference between two computed pressure coefficients is considerable, although their computed velocity profiles for this case also show good agreement with experiment. The difference

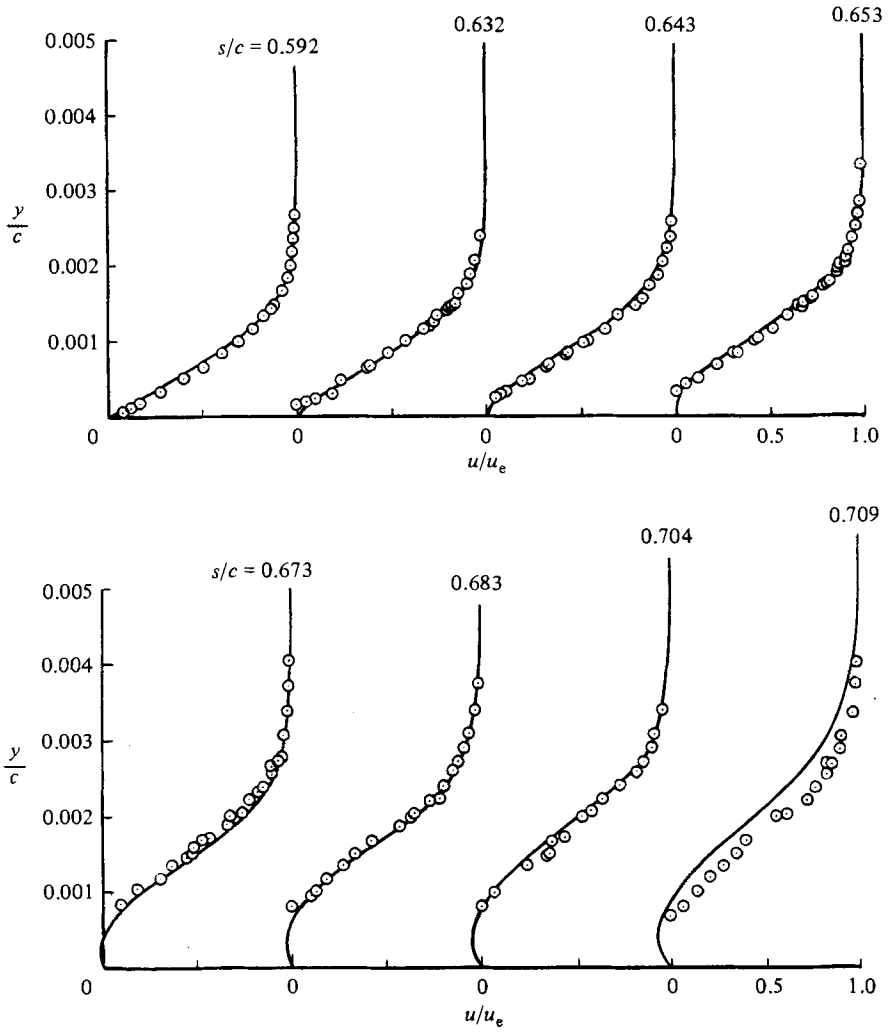

FIGURE 4. Comparison of calculated (solid line) and experimental (symbols) velocity profiles for $\alpha = 2$, $R_c = 2 \times 10^6$ after 15 sweeps.

Sweep	$(s/c)_{tr}$
1	0.67 (laminar separation)
2	0.68
3	0.68
4	0.67
5	0.67
6–9	0.66
10–19	0.67

TABLE 2. Variation of transition location for different sweeps for $\alpha = 2°$

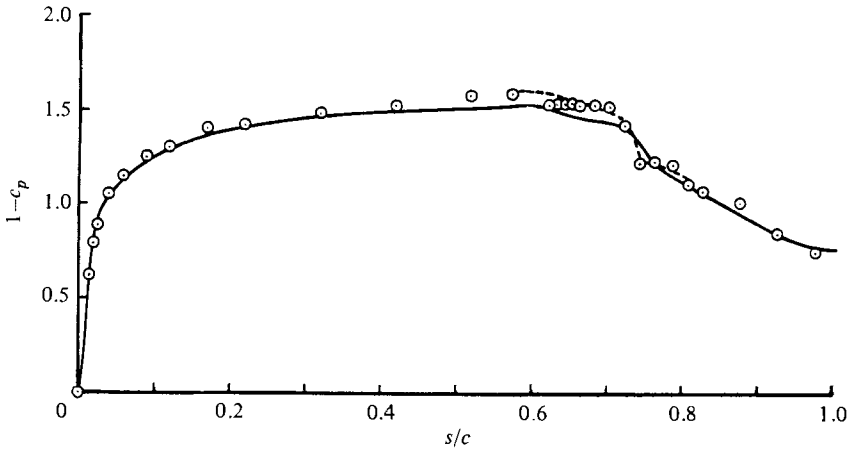

FIGURE 5. Comparison of calculated viscous (solid line) and measured (symbols) pressure coefficient for $\alpha = 0$, $R_c = 2 \times 10^6$. Calculation of Briley & McDonald (1975) (dashed line).

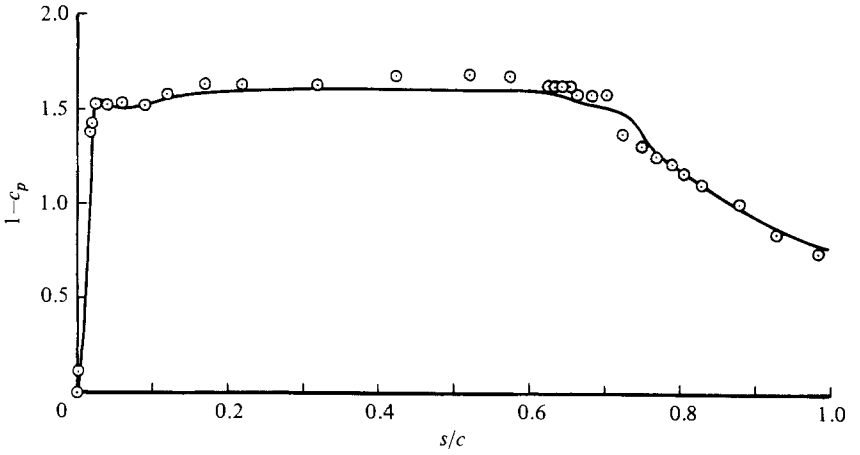

FIGURE 6. Comparison of calculated viscous (solid line) and measured (symbols) pressure coefficient for $\alpha = 2$, $R_c = 2 \times 10^6$.

between the present calculations and those observed by Briley & McDonald, however, can be attributed to the initial external velocity distribution used in both studies. While the present studies used a pressure distribution computed by an inviscid code due to Halsey, the studies of Briley & McDonald and also those by Kwon & Pletcher used the pressure distribution corresponding to $R_c = 10 \times 10^6$ measured by Gault (1955). A comparison between those pressure distributions and the ones computed by the inviscid code shown in figures 7 and 8 indicate considerable differences between them in the region where the velocity is nearly flat.

The principal conclusion to be drawn from the present study is the crucial role played by the choice of transition in determining the flow. Thus, if s_{tr} is fixed at $0.69c$, the iterations do not converge when $\alpha = 0$, whereas if it is fixed at $0.66c$, where laminar separation occurs, the inverse calculations do not contain a separated region. The choice of s_{tr} is clearly linked to that of the turbulence model, especially the intermittency factor γ_{tr}, and it is interesting that all three methods of computing the

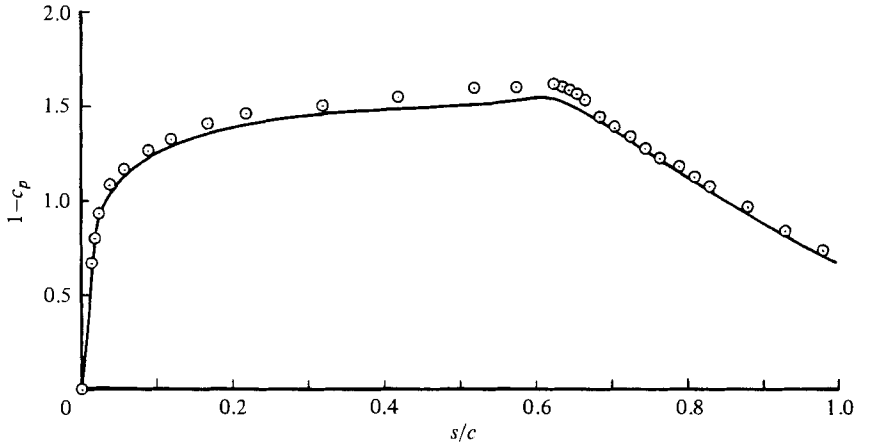

FIGURE 7. Comparison between measured (symbols) pressure coefficient at $R_c = 10 \times 10^6$ and inviscid calculation (solid line) for $\alpha = 0$.

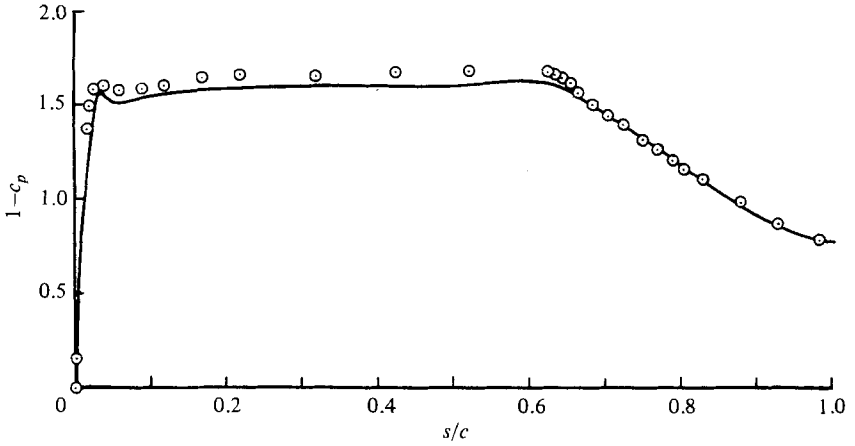

FIGURE 8. Comparison between measured (symbols) pressure coefficient at $R_c = 10 \times 10^6$ and inviscid calculation (solid line) for $\alpha = 2$.

flows compare with experiment in roughly the same ways. The velocity profiles correlate equally well and the separated region is shifted downstream by about the same amount. The primary cause for the discrepancy probably lies in the estimate of the laminar separation point, which is at $s = 0.66c$ when $\alpha = 0°$. The discrepancy between the pressure distributions computed according to inviscid theory and measured at $R = 10^7$ is surprising since it is confined to the central portion of the airfoil, the variations near the leading and trailing edges being in accord. In principle the same methods may be applied to study short bubbles near the leading edge of thin airfoils, and we hope to carry out this task in a later paper. It will be interesting to examine whether the formulaions we have been using have a more general validity and to compare their merits with the integral formulation of Crimi & Reeves (1976).

This research was supported under the National Science Foundation Grant MEA-8018565. The authors are grateful to Professor Keith Stewartson for his helpful comments and suggestions during the preparation of this manuscript.

REFERENCES

ARENA, A. V. & MUELLER, T. J. 1980 On the laminar separation, transition, and turbulent reattachment of low Reynolds number flows near the leading edge of airfoils. *AIAA J.* **18**, 747–753.

BRADSHAW, P., CEBECI, T. & WHITELAW, J. H. 1981 *Engineering Calculation Methods for Turbulent Flows.* Academic.

BRILEY, W. R. & MCDONALD, H. 1975 Numerical prediction of incompressible separation bubbles. *J. Fluid Mech.* **69**, 631–656.

BURSHALL, W. J. & LOFTIN, L. K. 1951 Experimental investigation of localized regions of laminar-boundary-layer separation. *NACA* TN2338.

CEBECI, T. & BRADSHAW, P. 1977 *Momentum Transfer in Boundary Layers.* Hemisphere/McGraw-Hill.

CEBECI, T. & SMITH, A. M. O. 1974 *Analysis of Turbulent Boundary Layers.* Academic.

CEBECI, T., STEWARTSON, K. & WILLIAMS, P. G. 1980 Separation and reattachment near the leading edge of a thin airfoil at incidence. *AGARD*-CP-291, Paper 20.

CHEN, K. K. & THYSON, N. A. 1971 Extension of Emmons' spot theory to flows on blunt bodies. *AIAA J.* **5**, 821.

CRIMI, P. & REEVES, B. L. 1976 Analysis of leading-edge separation bubbles on airfoils. *AIAA J.* **14**, 1548–1555.

GAULT, D. E. 1955 An experimental investigation of regions of separated laminar flow. *NACA* TN3505.

HALSEY, N. D. 1979 Potential flow analysis of multielement airfoils using conformal mapping. *AIAA J.* **17**, 1281–1288.

KWON, O. K. & PLETCHER, R. H. 1979 Prediction of incompressible separated boundary layers including viscous–inviscid interaction. *Trans. ASME* I: *J. Fluids Engng* **101**, 466–472.

TANI, I. 1964 Low-speed flows involving bubble separations. *Prog. Aero. Sci.* **5**, 70–103.

VELDMAN, A. E. P. 1979 A numerical method for the calculation of laminar incompressible boundary layers with strong-inviscid interaction. *NLR* TR79023L.